

Pendulums, Drops and Rods: a physical analogy

Benoît Roman¹, Cyprien Gay² and Christophe Clanet³

¹PMMH, UMR7636 du CNRS, ESPCI, 10 rue Vauquelin, 75005 Paris, FRANCE.

²MSC, UMR 7057 du CNRS, Université de Paris Diderot, France.

³LadHyX, UMR7646 du CNRS, Ecole Polytechnique, 91128 Palaiseau, FRANCE.

(Received 8 March 2024)

Abstract.

A liquid meniscus, a bending rod (also called elastica) and a simple pendulum are all described by the same non-dimensional equation. The oscillatory regime of the pendulum corresponds to buckling rods and pendant drops, and the high-velocity regime corresponds to spherical drops, puddles and multiple rod loopings. We study this analogy in a didactic way and discuss how, despite this common governing equation, the three systems are not completely equivalent. We also consider the cylindrical deformations of an inextensible, flexible membrane containing a liquid, which in some sense interpolates between the meniscus and rod conformations.

1. Introduction

Chapter LXXXIII of the Encyclopaedia Britannica (ninth edition) was written by JC Maxwell probably in the eighteenth century, as he was organizing the the new Cavendish Laboratory†. The whole article is 50 pages long, all dedicated to Capillary Action. Organized in 18 subchapters, the 7th is dedicated to the shape of a liquid meniscus on a wall:

The form of this capillary surface is identical with that of the “elastic curve”, or the curve formed by a uniform spring originally straight, when its ends are acted on by equal and opposite forces applied either to the ends themselves or to solid pieces attached to them. Drawings of the different forms of the curve may be found in Thomson and Tait’s Natural Philosophy, Vol.I, p 455.

This sentence has motivated the present work.

The power of the analogies in Physics is to enlight one subject using the known properties of its analogue. Here, pendulums, drops and rods are all classical subjects and the purpose is not to enlighten any one of the topics but to emphasize the properties shared by these three different systems.

2. The pendulum

A pendulum is presented on figure 1-(a). A particle of mass m moves under the gravitational acceleration g , remaining at a constant distance l from the fixed point o . The characteristic time of the system is:

$$\tau = \sqrt{l/g}. \quad (2.1)$$

† JC Maxwell died in 1879 at the age of 48 years.

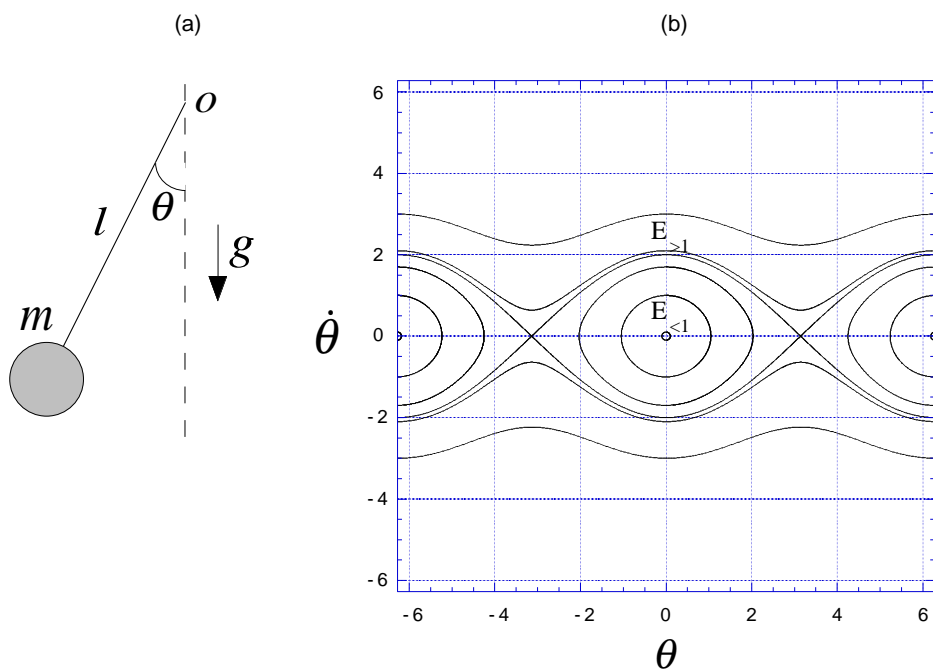


Figure 1. Pendulum: (a) sketch of the experiment, (b) Trajectories of the pendulum in the $[\theta, \dot{\theta}]$ phase diagram.

Denoting by θ the angle between the vertical and the pendulum, the non-dimensional equation of motion reads:

$$\frac{d^2\theta}{dt^2} = -\sin\theta. \quad (2.2)$$

The minus sign is changed to a plus sign when gravity is reversed. Equation (2.2) is then recovered in its original form through the translation $\theta \rightarrow \theta + \pi$. Equation (2.2) is thus generic for the pendulum, whatever the direction of the gravity field. The first integral of motion of this equation corresponds to the conservation of the total energy (in units of mgl):

$$E \equiv \frac{1}{2}\dot{\theta}^2 - \cos\theta \quad (2.3)$$

The trajectories obtained with different energy values are presented in the phase diagram $[\theta, \dot{\theta}]$ on figure 1-(b). Two different regions appear: a region with closed orbits, denoted by $E_{<1}$, where the total energy is smaller than unity, and a region with open trajectories, $E_{>1}$, where the total energy is larger than unity. The main difference between both regions is the existence on the trajectories of points with vanishing angular speed $\dot{\theta}$ in the region $E_{<1}$, and their absence in the region $E_{>1}$. We will see later that these points correspond to inflexion points on the shape of a rod, or of a drop. The special case $E = 1$ (separatrix) defines the soliton motion and will be addressed separately in section 5.

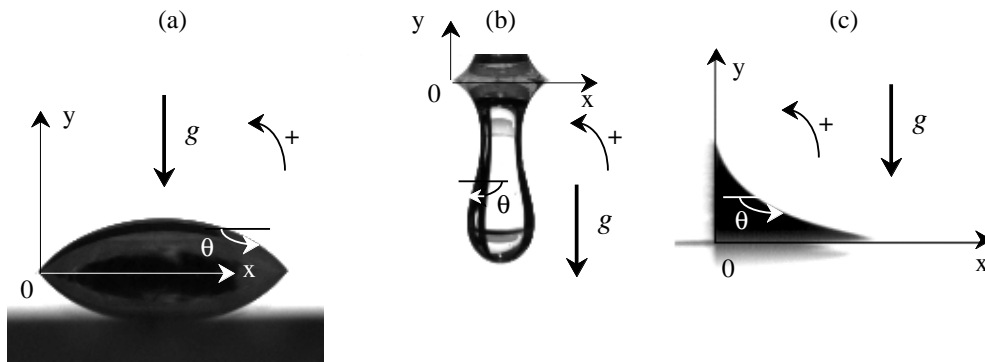


Figure 2. 2D drops and meniscus: (a) drop compressed by gravity and its image reflected on the substrate, (b) pendant drop stretched by gravity, (note the different convention for measurement of angle θ in this case, which allows to keep the same equations throughout the article) (c) meniscus near a solid wall.

3. Drops and bubbles

In this section, we consider the shapes of 2D static drops[†], either compressed (figure 2-(a)), or stretched by gravity (figure 2-(b)). The 2D meniscus presented in figure 2-(c) will be discussed in section 5. In these three cases, the shape of the interface results from the equilibrium between surface tension, σ , and gravity, g . We describe this equilibrium with the notations and conventions presented in figure 2. Note that the definition adopted for θ is different for drops compressed by gravity (and the special case of meniscus) and for drops stretched by gravity. With these conventions, we will deal with the same equation throughout our discussion. In the three cases, θ is measured through the liquid from the horizontal to the tangent.

The equilibrium shape of a bubble blocked beneath a solid surface (resp. anchored to a solid) can be mapped, through reflection by a horizontal plane, onto that of a liquid drop resting on a plane (resp. a pendant drop). Indeed, gravity and density difference are both reversed through this symmetry. In this section, we will therefore simply focus on drops.

3.1. Drops on a solid surface.

The shape of a liquid drop resting on a solid surface is characterized by its volume, \mathcal{V} , and the contact angle, $\theta_e \in [0, \pi]$ between the free surface and the solid. Small contact angles correspond to good wetting (if the contact angle is zero, wetting is said to be complete), while large contact angles are observed for poor wetting or non-wetting situations. Three drops of mercury on plexiglass ($\theta_e \approx \pi$), are presented in figure 3. As the volume is increased, the shape changes from an almost perfect circle (figure 3-(a)) to a puddle (figure 3-(c)).

To account for the shape, we express the pressure at a given point located behind the interface at altitude y in two ways, following the paths (1) and (2) indicated on figure 3-(c). The pressure, p , beneath the interface is larger than the ambient pressure, p_0 , due to surface tension, as can be seen from figure 4. When the free surface is curved, the force associated to surface tension is tangent to the surface and changes directions from place to place. As a result, the force is not balanced on both sides of a curved section of the surface. Hence, it exerts a pressure towards the center of curvature ($-\vec{n}$ direction), which results in a pressure difference between the liquid and the gas, called the Laplace

[†] 2D is used to designate shapes with one curvature. Axisymmetric shapes are thus not included and will be discussed in section 3.3.

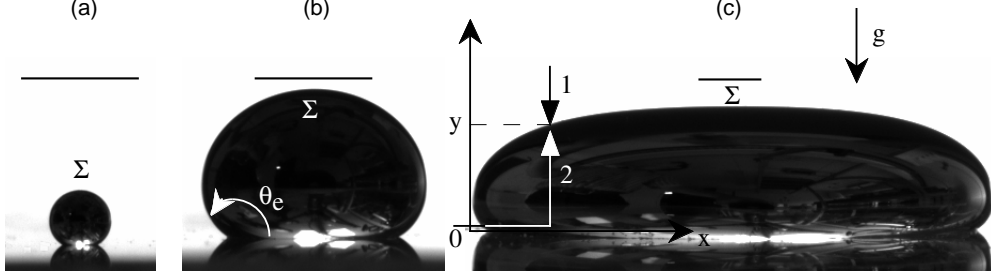


Figure 3. Drops of mercury on plexiglass ($\theta_e \approx \pi$), with different volumes: (a) $\mathcal{V} = 0.35 \text{ mm}^3$, (b) $\mathcal{V} = 12.9 \text{ mm}^3$, with θ_e is the contact angle, (defined with standard angle convention) (c) $\mathcal{V} = 426.5 \text{ mm}^3$, (the horizontal bar on each picture represents 1.7 mm).

pressure, Δp_L , which is proportional to the total curvature of the surface:

$$\Delta p_L = \sigma \left(\frac{1}{R_1} + \frac{1}{R_2} \right). \quad (3.1)$$

where R_1 and R_2 are the principal radii of curvature. In figure 4, R_1 and R_2 are both positive and surface tension imposes that the pressure in the liquid is higher than in the air. In a two-dimensional situation where the shape is invariant in one direction, one principal radius of curvature is infinite, and the total curvature is simply equal to the curvature of the curve in the perpendicular cross-section. Laplace's equation thus yields the pressure p following path (1):

$$p = p_0 - \sigma \frac{d\theta}{ds}, \quad (3.2)$$

where p denotes the pressure in the liquid, and s is a curvilinear coordinate. In this equation, $d\theta/ds$ is the local curvature of the interface. Following path (2), the pressure contains also a hydrostatic term:

$$p = p_0 - \sigma \left(\frac{d\theta}{ds} \right)_0 - \rho g y, \quad (3.3)$$

where ρ is the density of the liquid, y is the altitude and $\left(\frac{d\theta}{ds} \right)_0$ is the curvature at height $y = 0$. From equations (3.2) and (3.3):

$$\frac{d\theta}{ds} = \left(\frac{d\theta}{ds} \right)_0 + \frac{y}{a^2}, \quad (3.4)$$

where the characteristic length scale

$$a \equiv \sqrt{\sigma/(\rho g)} \quad (3.5)$$

is the capillary length. Non-dimensionalization by a and differentiation with respect to s yields the pendulum equation (2.2):

$$\frac{d^2\theta}{ds^2} = -\sin \theta, \quad (3.6)$$

where the geometrical relation $dy/ds = -\sin \theta$ has been used. As compared to equation (2.2), the time derivative of the pendulum equation has been replaced by the spatial derivative along the surface, and the characteristic time $\tau = \sqrt{l/g}$ has been replaced by the characteristic length $a = \sqrt{\sigma/(\rho g)}$. Since both phenomena share the same non-

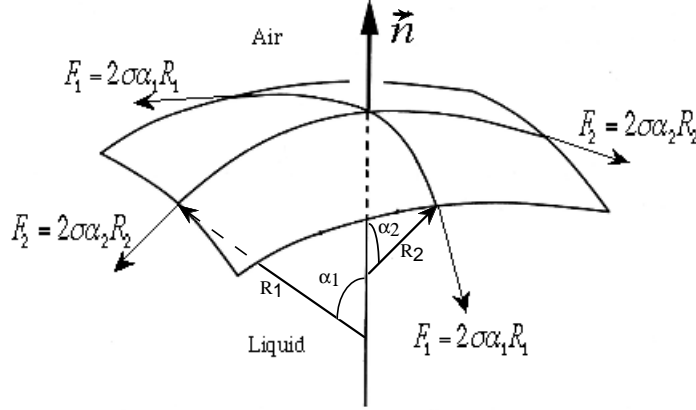


Figure 4. Illustration of the Laplace pressure jump Δp_L across a curved interface. We consider a small element of surface whose principal radii of curvature are R_1 and R_2 and which spans an infinitesimal angle $2\alpha_1$ in one direction and $2\alpha_2$ in the other direction, as seen from the centers of curvature. Let $F_1 = 2\sigma\alpha_1 R_1$ is the force due to the surface tension σ acting on one edge of length $2\alpha_1 R_1$. It is oriented at angle α_2 from the tangent plane to the surface. Its normal component is thus $F_1 \sin \alpha_2 \approx F_1 \alpha_2$. Including the opposite edge and the similar contribution from F_2 , we obtain $\Delta p_L \cdot 2R_1 \alpha_1 \cdot 2R_2 \alpha_2 = 4\alpha_1 \alpha_2 \sigma (R_1 + R_2)$, which justifies the expression of the Laplace pressure jump Δp_L given by equation (3.1).

dimensional equation, their phase diagrams are also identical. The total energy,

$$E \equiv \frac{1}{2} \dot{\theta}^2 - \cos \theta \quad (3.7)$$

(which is the same as equation (2.3) for the pendulum), can be evaluated at the apex, Σ , indicated on figure 3. By symmetry, $\theta_\Sigma = \pi$, so that $E = 1 + \dot{\theta}_\Sigma^2/2$. For all the drops lying on a solid surface, the energy E is thus larger than unity so that the corresponding trajectories always lie in the $E_{>1}$ region, where no inflection point are present (the curvature, $\dot{\theta}$, does not vanish).

Figure 5-(a) shows the shapes obtained through the numerical integration of equation (3.6), with $\theta(0) = 2\pi$ and different energies, E , chosen so as to give the same aspect ratio as the drops presented in figure 3. The corresponding trajectories in the phase diagram $[\theta, \dot{\theta}]$ are presented in figure 5-(b). The puddle approaches the separatrix defined by $E = 1$, whereas the small circular drop corresponds to the high energy region. The limit of circular drops corresponds to the high energy pendulum, where gravity almost does not affect the momentum of the pendulum. With the conventions adopted on figure 2-(a), the trajectory of one drop extends from $\pi - \theta_e$ to $\pi + \theta_e$ (that is from 0 to 2π with mercury on plexiglass) and $\dot{\theta}$ is negative, so that all the drops are contained in the south-east region of the phase diagram indicated with symbols in figure 5-(b). It is easy to show that with different conventions keeping the equation (3.6) unchanged, the other three regions (SW, NW and NE) can be reached, one at a time. In all cases, the trajectory is symmetrical with respect to the vertical line $\theta = \theta_\Sigma$, where θ_Σ corresponds to the apex of the drop. At this point θ_Σ , the curvature $|\dot{\theta}|$ is minimal, due to the direction of gravity. It clearly follows that $\theta_\Sigma = \pi$ modulo 2π .

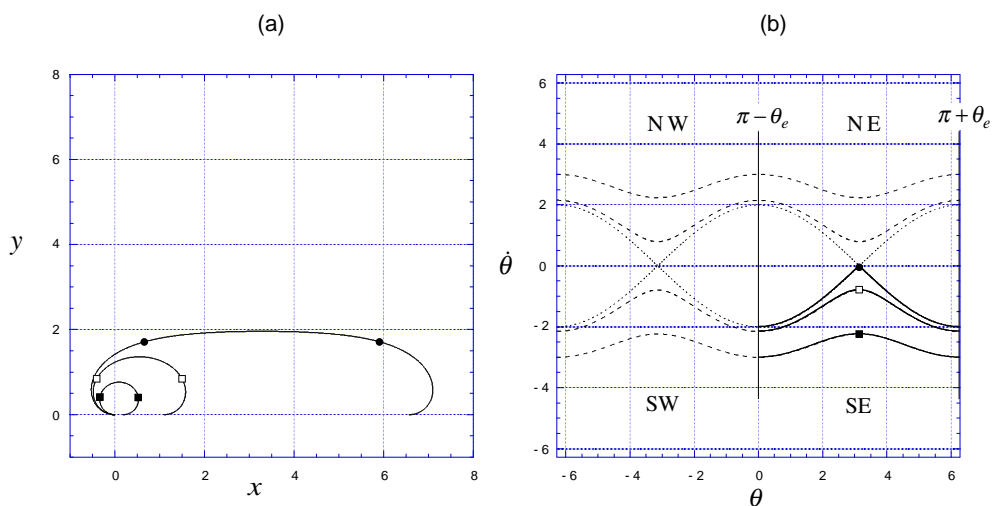


Figure 5. Numerical integration of equation (3.6), with $\theta(0) = 2\pi$ and different energies, \blacksquare $E = 3.5$, \square $E = 1.3$, \bullet $E = 1.007$: (a) shape of the drops, (b) phase diagram. Note that the \bullet curve does not correspond exactly to the separatrix ($E = 1$) for which the drop would have an infinite lateral extension (infinite puddle).

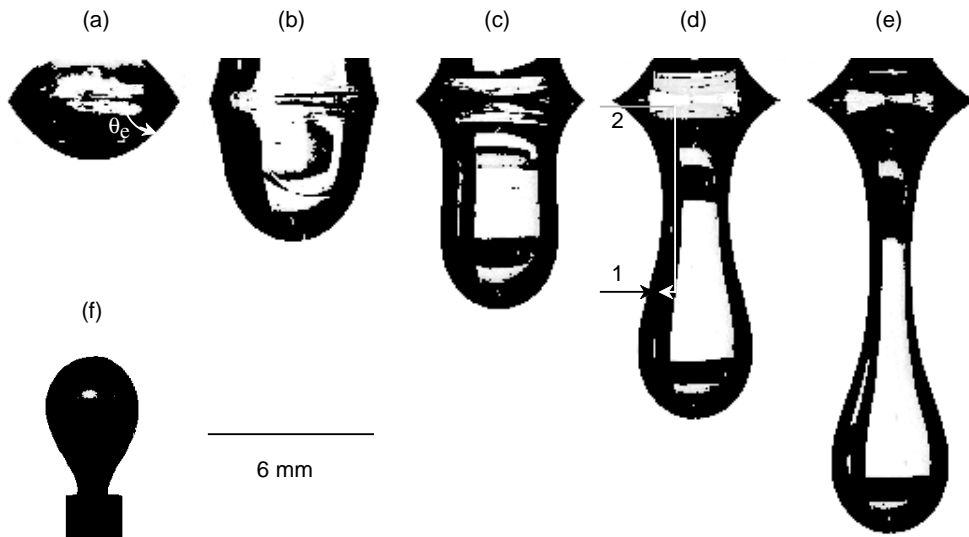


Figure 6. Drops and bubble. Drops of glycerine under plexiglass with different volumes: (a) $\mathcal{V} = 31 \text{ mm}^3$ (contact angle θ_e presented with usual angle definition), (b) $\mathcal{V} = 82 \text{ mm}^3$, (c) $\mathcal{V} = 95 \text{ mm}^3$, (d) $\mathcal{V} = 95 \text{ mm}^3$, (e) $\mathcal{V} = 95 \text{ mm}^3$. (f) Anchored air bubble stretched by buoyancy in water. The last three drops (c-e) are actually slowly deforming over time. Their shapes are therefore not defined by the static equation, since viscous stresses are involved.

3.2. Drops under a solid surface and pending drops.

Figure 6 shows drops of glycerine hanging from a plexiglass surface (contact angle $\theta_e \approx 55^\circ$). The reflection on the plate allows for a precise determination of both the angle of contact and the position of the surface. Such three-dimensional drops or bubbles are described by a slightly more complex equation (see (3.10) in the next paragraph) than

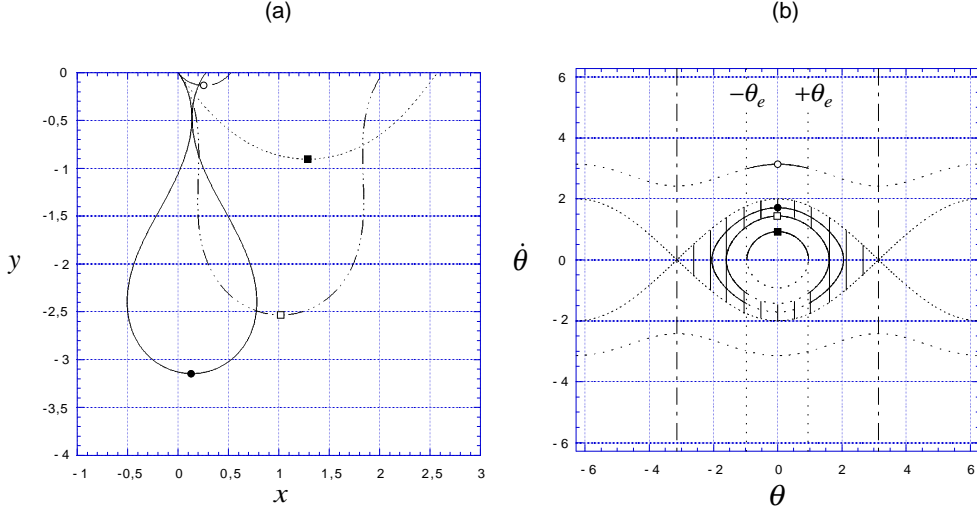


Figure 7. Shapes obtained from equation (3.6) with $\theta(0) = -\theta_e = -55^\circ$ and different energy values, \blacksquare $E = -0.57$, \square $E = 0.027$, \bullet $E = 0.468$, \circ $E = 3.92$: (a) Shapes in real space (b) Corresponding trajectories in phase space. The dashed region is forbidden because 2D drops would include a larger volume than allowed by gravity.

the 2D equation that we shall now derive. With the conventions[†] of figure 2-(b), the pressure at a given point beneath the interface can be expressed in two ways (paths (1) and (2) of figure 6-d). Through path (1), we get:

$$p = p_0 + \sigma \frac{d\theta}{ds}, \quad (3.8)$$

and through path (2):

$$p = p_0 + \sigma \left(\frac{d\theta}{ds} \right)_0 - \rho g y. \quad (3.9)$$

Upon non-dimensionalisation by the capillary length and differentiation with respect to the curvilinear distance s , we recover the pendulum equation (3.6), since $dy/ds = \sin \theta$ in this case. Figure 7-(a) shows four shapes obtained from equation (3.6) with $\theta(0) = -\theta_e$ and different values of the energy. The corresponding trajectories in the phase diagram $[\theta, \dot{\theta}]$ are presented in figure 7-(b). These trajectories extend from $-\theta_e$ to $+\theta_e$, and some of them have an inflection point. Due to the orientation of gravity, $|\dot{\theta}|$ is maximal on the axis of symmetry, which implies that it is located at $\theta = 0$ modulo 2π . Note that the anchored bubble (figure 6-(f)) is the symmetric counterpart of the pendant drop.

Pendant drops cannot exceed some maximal volume, \mathcal{V}_{max} , beyond which capillarity is unable to sustain their weight. The volume of the drop presented on figures 6-(c-e) is actually larger than \mathcal{V}_{max} : these three images represent the same drop at different times. Their shapes cannot be understood solely with static arguments and are affected by viscous stresses.

The exact value of \mathcal{V}_{max} or, in more general terms, the maximum value of the energy E for a pendant drop depends in a subtle way on both the geometry of the sustaining solid and the imposed condition (such as fixed drop volume or fixed pressure at a given

[†] Note that the definition of angle θ used in this section and in figure 2-(b) is related to that of figure 2-(a) by $\theta \rightarrow \pi + \theta$. This allows to use the same equation for all systems in the article.

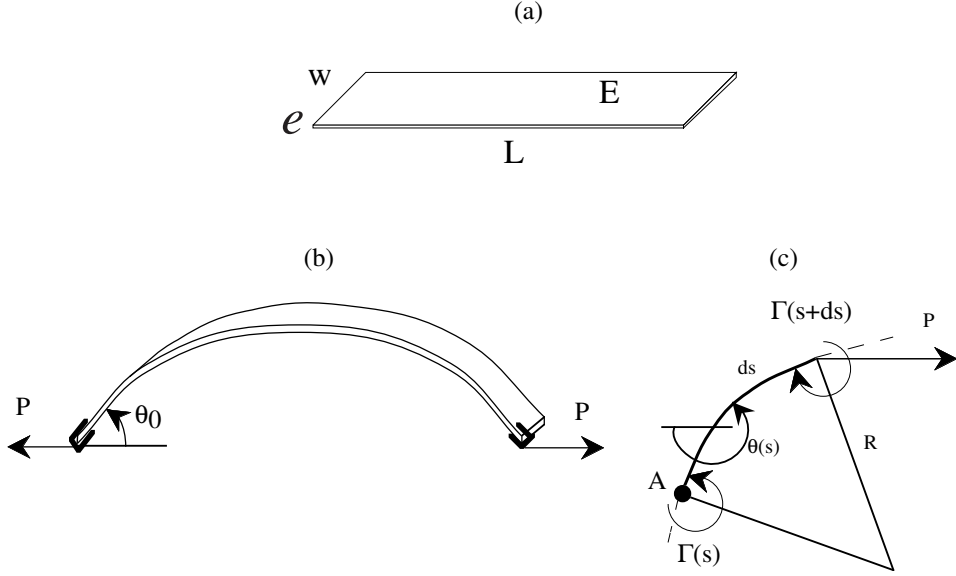


Figure 8. Experiment with a rod: (a) characteristic parameters of the rod, (b) rods subject to extension (outbound forces P), (c) local torque balance and angle definition.

altitude, for instance). For instance, as shown in a detailed analysis by Majumdar and Michael [9], a two-dimensional drop anchored to two parallel edges located at the same altitude destabilizes through three-dimensional perturbations at a smaller volume than it would through two-dimensional ones if the pressure is held constant at the anchoring edges. Another contribution to the stability of capillary surfaces can be found in [8].

Conversely, the stability threshold for both types of perturbations is the same (and hence higher) if the volume of the drop is fixed.

3.3. Three-dimensional drops.

To conclude this section dedicated to 2D drops (whose shape is invariant in one direction), let us mention that usual, 3D drops exhibit axial symmetry and the azimuthal curvature of the surface cannot be neglected in general. In the case of a drop on a solid, equation (3.6) is changed into:

$$\frac{d^2\theta}{ds^2} = -\sin\theta + \frac{d}{ds} \left(\frac{\sin\theta}{x_\Sigma/a} \right), \quad (3.10)$$

where x_Σ is the horizontal distance of the current point to the axis of symmetry of the drop and a is still the capillary length. This equation clearly reduces to equation (3.6) for large values of x_Σ/a , i.e., for the edge of a puddle (which is essentially the same as that of a 2D puddle). For small drops ($x_\Sigma/a < 1$), the 2D equation we have used is only in qualitative agreement with the observed shape. In the same way, the exact equation for an axisymmetrical suspended drops is:

$$\frac{d^2\theta}{ds^2} = -\sin\theta - \frac{d}{ds} \left(\frac{\sin\theta}{x_\Sigma/a} \right). \quad (3.11)$$

A detailed study of these axisymmetrical capillary surfaces is presented in [7].

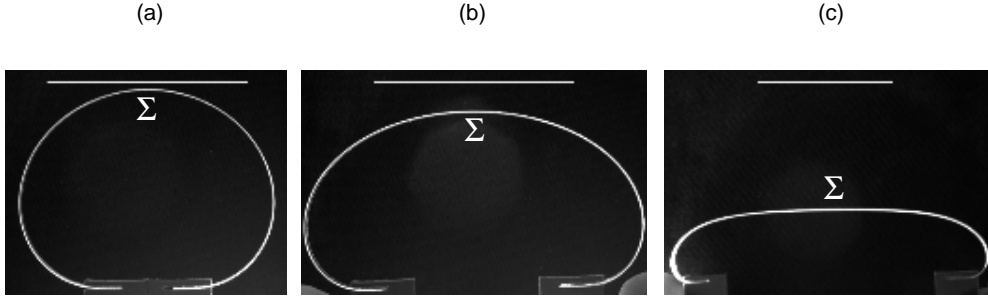


Figure 9. Examples of extended rods (increasing extension from a to c) obtained with $\theta_0 = \pi$ (the horizontal bars are 8 cm long).

4. Flexible rod

We now move to the flexible rod problem, depicted on figure 8-(a). The rod is characterized by its length, L , thickness, e , width, w , and Young modulus, Y . Introducing the moment of inertia $I \equiv we^3/12$ with respect to the mid-plane, we now consider the rod as a massless, inextensible line of bending rigidity $\mu \equiv YI$. Here again we will study two cases (rod under tension or compression) with two different geometric conventions.

4.1. Rod subjected to a traction force P .

Let us first consider that the rod is clamped at both ends in symmetrical stirrups. Let us impose some initial angle, θ_0 , and a horizontal force, P , as depicted on figure 8-(b). Figure 9 presents the shape of a polycarbonate sheet ($\mu = 5.10^{-4} \text{kg.m}^3.\text{s}^{-2}$) subjected to various forces P (increasing from left to right) with $\theta_0 = \pi$. These shapes are similar to those obtained with Mercury drops on a solid (see figure 3). According to d'Arcy approach [1], this suggests that they both share the same equation. Since the rod is not subjected to any body forces (negligible weight), the local force balance on a small element ds of the rod is trivial: $P(s) = P(s + ds) = P$. The torque balance, however, is not. With the conventions of figure 8-(c) (note that θ is defined exactly as in the case of a resting drop in figure 2-(a)), it can be written as:

$$\Gamma(s + ds) - \Gamma(s) + Pds \sin \theta = 0, \quad (4.1)$$

where $\Gamma(s)$ is the torque applied by the right-hand side part of the rod (abscissa larger than s) onto the left-hand side part of the rod (abscissa smaller than s). Its value was related, by Euler [12], to the radius of curvature R , through the relation $\Gamma(s) = \mu/R(s) = \mu d\theta/ds$. Equation (4.1) thus reads:

$$\frac{d^2\theta}{ds^2} = -\sin \theta, \quad (4.2)$$

where the characteristic length

$$a_e \equiv \sqrt{\mu/P} \quad (4.3)$$

has been used for the non-dimensionalization. The energy of the rod trajectory is given by:

$$E = \frac{1}{2} \dot{\theta}^2 - \cos \theta \quad (4.4)$$

(see equations (2.3) and (3.7) for comparison). By symmetry $\theta_\Sigma = \pi$ at the middle point, Σ , and the energy can be evaluated as $E = 1 + \dot{\theta}_\Sigma^2/2$. Rods subject to outbound forces P (as in figure 8-(b)) are thus confined in the high energy region, $E_{>1}$. Moreover, according

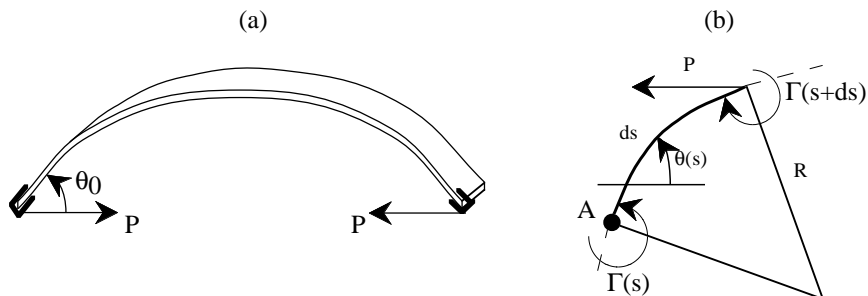
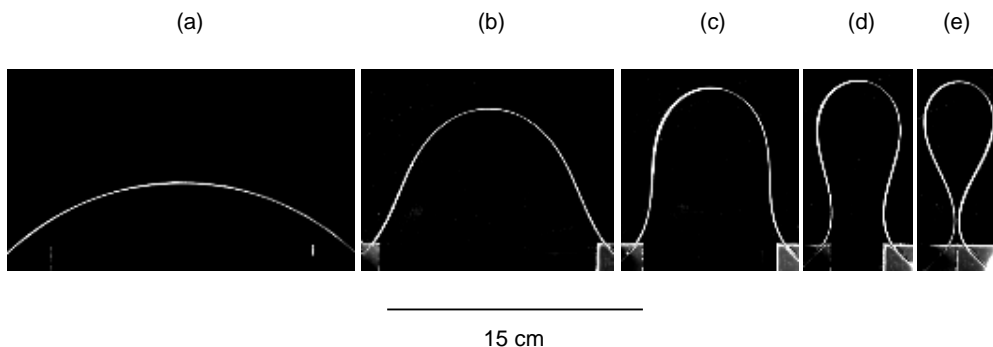


Figure 10. Compressed rod: (a) sketch of the experiment, (b) local torque balance.

Figure 11. Examples of compressed rods obtained with $\theta_0 = \pi/4$, the compression increases from (a) to (e).

to equation (4.2), $|\dot{\theta}|$ reaches an extremum when $\theta = \pi$. The puddle-like shape shown on figure 9-(c) indicates that this extremum is a minimum. The trajectories of extended rods are thus symmetrical with respect to $\theta = \pi$ modulo 2π . They are strictly analogous to the drops on a solid, the capillary length being replaced by the elastic length a_e , and the contact angle by the clamping angle. It can be observed that this length can be changed at will, by varying either μ or P . This is not the case with liquids on Earth, since a is typically confined within the range 1 mm – 5 mm.

4.2. Rod submitted to a compressive force P .

The clamped rod is now compressed by a force P (see figure 10). The shapes observed experimentally with the polycarbonate sheet ($\mu = 5.10^{-4} \text{kg.m}^3.\text{s}^{-2}$) are presented on figure 11 when subjected to an increasing compression, keeping all other parameters constant. These shapes are similar to those obtained with suspended drops (figure 6). With the conventions of figure 10-(b), which are the same as those for the pendant drop in figure 2-b, the torque balance reads:

$$\Gamma(s + ds) - \Gamma(s) + Pds \sin \theta = 0, \quad (4.5)$$

which yields the pendulum equation (4.2) upon using the elastic length a_e and the Euler relation $\Gamma = \mu d\theta/ds$. At the middle point, $\dot{\theta}$ is now a maximum, which means that the trajectory is symmetric with respect to $\theta = 0$ modulo 2π . The inflection points, observed for example on figure 11-(e), show that we have now access to the region $E_{<1}$: compressed rods are thus strictly similar to suspended drops. The forbidden region resulting from the gravitational constraint does not exist in this case.

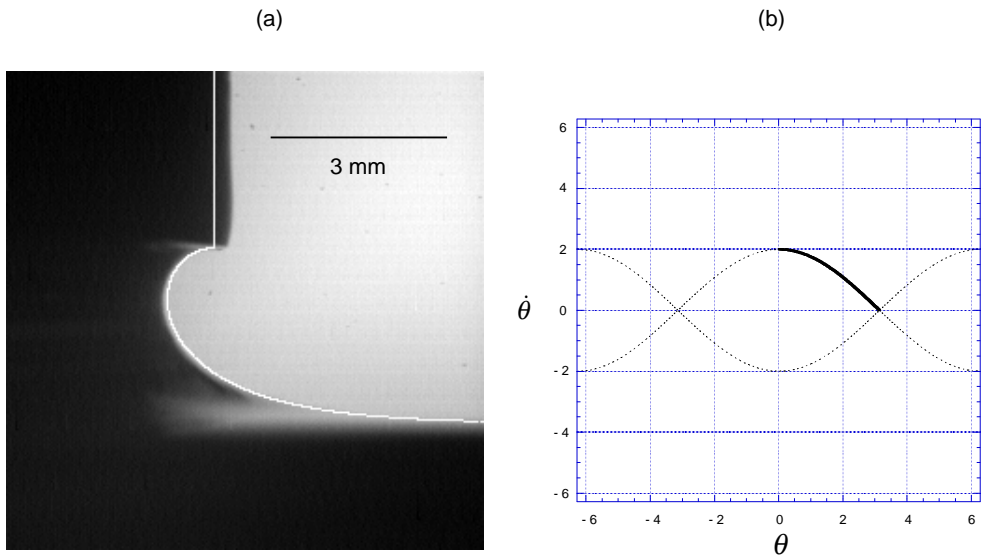


Figure 12. Shape of the meniscus: (a) comparison between the algebraic equation (5.2) and a meniscus of silicone oil V1000, located under a column of large cross-section (diameter $D = 20$ mm), (b) corresponding trajectory in the phase diagram $[\theta, \dot{\theta}]$.

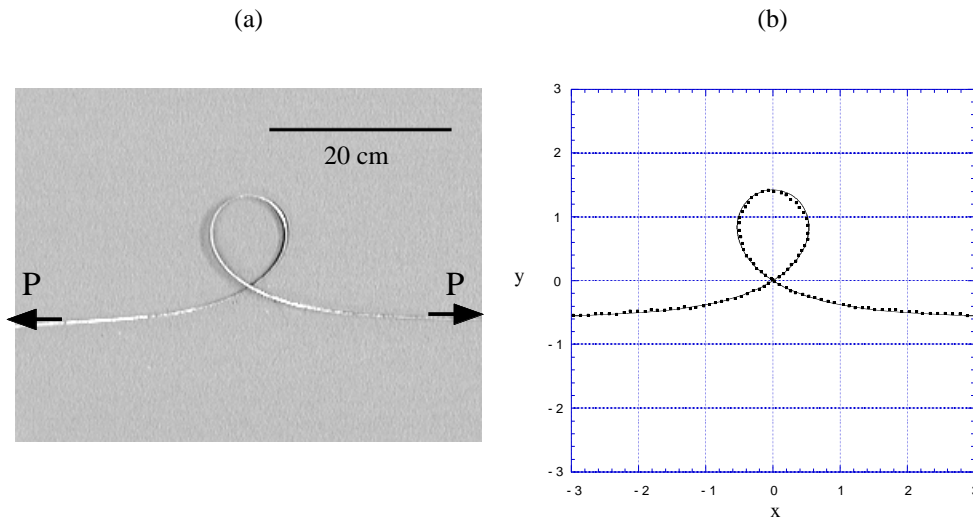


Figure 13. Meniscus-shaped elastica: (a) Stainless steel saw blade. (b) Experimental shape (dots) and plot (full curve) of the algebraic equation (5.2).

5. Menisci, looping and soliton

In the previous sections we have focused our attention on both generic behaviors of all three systems, which are characterized by closed orbits (energy $E < 1$) or open trajectories ($E > 1$) in the $[\theta, \dot{\theta}]$ diagram. To illustrate the analogy more deeply, we now describe the particular behavior that corresponds to the separatrix, $E = 1$.

As opposed to the rotation motion ($E > 1$) or the oscillating regime ($E < 1$), the particular motion of the pendulum obtained when it is dropped with vanishing velocity from

its unstable equilibrium position is not periodic in time: the pendulum slowly accelerates, then passes through its lowest position at full speed and moves up again slowly, until it finally stops at its uppermost position again. On the $[\theta, \dot{\theta}]$ diagram, this trajectory has two ends located in a bounded region, which is not the case for all other trajectories. Moreover, most of the motion occurs during a finite time interval. This particular motion is therefore a solitary excitation of the pendulum: it is sometimes called the soliton motion, although this term usually rather designates localized, travelling waves that exist in many non-linear media.

The corresponding shape for a liquid is the most usual occurrence of a meniscus, namely the curved region of the free surface in the vicinity of the container wall, see figure 2-(c). It results from the fact that because of the local surface tension balance, the free surface has to meet the solid surface with a fixed angle (known as the contact angle, θ_e). The dimension of the container is usually much larger than the capillary length a , which implies that both $\theta - \pi$ and the curvature $\dot{\theta}$ vanish far from the walls. This indeed yields $E = 1$ according to equation (3.7). This equation can be integrated exactly in this particular case:

$$\sin \frac{\theta}{2} = \tanh s \quad (5.1)$$

where the origin of the curvilinear distance is taken at the apex of the looping ($\theta = 0$). It can also be integrated exactly in cartesian coordinates [10]:

$$\frac{1}{2} \ln \left(\frac{1 + \sqrt{1 - y^2/4}}{1 - \sqrt{1 - y^2/4}} \right) - 2\sqrt{1 - y^2/4} = x. \quad (5.2)$$

This function is plotted on figure 12-(a) and compared to a meniscus of silicone oil V1000 located under the edge of a column of diameter $D = 20$ mm. The meniscus is essentially two-dimensional since the column diameter is much larger than the capillary length. The corresponding trajectory in the phase diagram is presented in figure 12-(b).

The corresponding elastic conformation is that of a very long flexible rod with one single curl, loaded by a pure force at each end (no applied torque).

On figure 13-(a), we present a meniscus shape formed with a stainless steel saw blade ($\mu = 5.10^{-2} \text{kg.m}^3.\text{s}^{-2}$), submitted to a traction force $P = 10$ N (which corresponds to $a_e \approx 7$ cm). On figure 13-(b), this looping is shown to be in nice agreement with the algebraic equation (5.2).

6. How deep is the analogy?

In the preceding sections, we presented the analogy between all three systems essentially through the equation that describes them. Figure 14 illustrates the variety of shapes that can be obtained in principle.

In this section, in order to show a more precise physical correspondence between the different actors in these analogies, we first present a variational approach of each system, which shows that although the equation of motion is the same, the energy is somewhat different. We then discuss an instability which is similar for the meniscus and for the flexible rod. We present the pendulum counterpart of the instability, which displays some dissimilarities with the other two. We finally briefly study the behavior of a flexible membrane enclosing a liquid, which interpolates between the elastic rod and the meniscus. The table in figure 15 summarizes several aspects of the analogy.

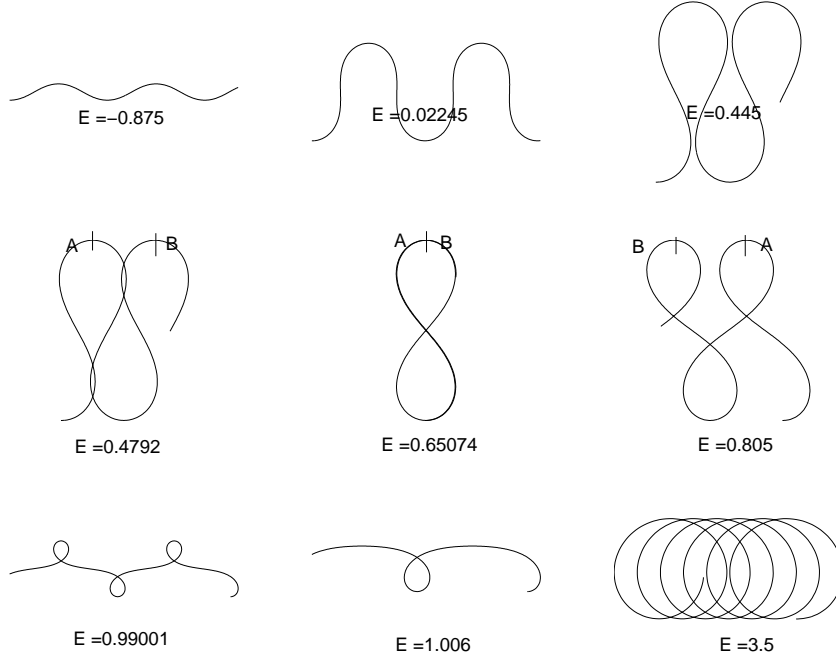


Figure 14. Various possible shapes obtained from the pendulum equation for different values of the pendulum energy E . Some of these shapes can be materialized with a meniscus or an elastica. (a) E slightly larger than -1 corresponds to gentle undulations; (b) for $E \simeq 0.02245$, vertical slopes are reached; (c-d) for $E \approx 0.46$, the curve now intersects itself: an elastica needs to be thin enough (thread) for crossings not to distort it too much in the third direction; (e) for $E \approx 0.65074$, the curve is continuously self-superimposed (8-shape); (f) for values of E larger than about 0.65074 , loops are formed; correlatively, if the conventions for plotting the curve are preserved, the overall motion along the curve is reversed as compared to smaller values of E , as seen from the positions of points A and B ; (g) as E is further increased, the loops are located further apart and are still alternatively pointing up and down; (h) beyond the soliton solution $E = 1$ for which only one looping is present, the loops are now all pointing in the same direction; (i) for high values of E , successive loopings come close together and intersect.

6.1. Variational description

Comparing the governing equation, as we have done so far, shows a deep similarity between all three systems. Among them, the meniscus and the elastic rod are most similar since the variable s has the same spatial meaning: we now turn to a variational approach of these two systems, in the case of the pendant drop, and of the compressed rod for simplicity.

For the liquid, the following quantity needs to be minimized:

$$\int_0^X \mathcal{L}(y, y') dx, \quad \text{where} \quad \mathcal{L} = -\frac{1}{2} \rho g (y - y_0)^2 + \sigma \sqrt{1 + y'^2}, \quad (6.1)$$

where the first term is the gravitational potential energy of the liquid column located above each point of the interface with respect to some reference altitude y_0 and where the second term is the interfacial energy. The full Euler-Lagrange equation reads:

$$\frac{\sigma}{R} + \rho g (y - y_0) = 0, \quad (6.2)$$

where $1/R = \dot{\theta} = y''/(1 + y'^2)^{3/2}$ is the surface curvature. This relation was found

(Eqs.) in text	Pendulum	Drops	Flexible rod
parameters	angle θ time t velocity $\dot{\theta}$	angle θ curv. distance s curvature $\dot{\theta}$	angle θ curv. distance s curvature $\dot{\theta}$
characteristic scale (2.1) (3.5) (4.3)	$\tau = \sqrt{\frac{l}{g}}$ length l , gravity g	$a = \sqrt{\frac{\sigma}{\rho g}}$ surface tension σ density ρ	$a_e = \sqrt{\frac{\mu}{P}}$ applied force P bending rigidity μ
simplest governing eq. (2.2) (3.4) (6.9)	angular acceleration due to gravity $ml\ddot{\theta} = -mg \sin \theta$	$\sigma\dot{\theta} = -\rho g y$ pressure	$\mu\dot{\theta} + P y = 0$ torque
conserved "energy" E (2.3) (3.7) (4.4)	$\frac{1}{2}ml^2\dot{\theta}^2 - mgl \cos \theta$	$\frac{1}{2}\rho g y^2 - \sigma \cos \theta$	$\frac{1}{2}\mu\dot{\theta}^2 - P \cos \theta$
$E < 1$ $E > 1$ $E = 1$	oscillations rotations soliton	$\left. \begin{array}{l} \text{Drops and bubbles} \\ \text{bounded by} \\ \text{angle with} \\ \text{solid surface} \end{array} \right\}$ 2D meniscus	compressed stretched single looping
unperturbed state perturbation instability threshold	$\theta(t) = \pi$ (unstable equil.) angular frequency ω $\omega \cdot \tau < \mathcal{O}(1)$	$\theta(s) = 0$ (liquid above air) wavenumber k Rayleigh-Taylor $k \cdot a < \mathcal{O}(1)$	$\theta(s) = 0$ (compressed) wavenumber $k = 2\pi/L$ Euler buckling $k \cdot a_e < \mathcal{O}(1)$

Figure 15. Comparison of the different systems

in section (3.2). Upon differentiation with respect to s we again find the pendulum equation (4.2):

$$\sigma \ddot{\theta} + \rho g \sin \theta = 0 \quad (6.3)$$

A first integral can be obtained as $y' \partial \mathcal{L} / \partial y' - \mathcal{L} = \text{const}$:

$$\frac{1}{2} \rho g (y - y_0)^2 - \sigma \cos \theta = \text{const} \quad (6.4)$$

(where $\cos \theta = 1/\sqrt{1 + y'^2}$). When combined with equation (6.2), this yields the energy (see equation (3.7) for comparison):

$$E = \frac{1}{2} \dot{\theta}^2 - \cos \theta \quad (6.5)$$

where s has been rescaled by $a = \sqrt{\sigma/(\rho g)}$.

The rod energy per unit length is $\frac{1}{2}\mu\dot{\theta}^2$. Enforcing a prescribed value for the horizontal distance $\int \cos \theta ds$ swept by the entire rod of length L , yields an additional term in the energy to be minimized:

$$\int_0^L \mathcal{L}(\theta, \dot{\theta}) ds \quad \text{where} \quad \mathcal{L} = \frac{1}{2} \mu \dot{\theta}^2 + P \cos \theta \quad (6.6)$$

where the Lagrange multiplier P is the force (assumed to be horizontal) applied at both

ends of the rod. The above integral can be interpreted as the action, where the first term in \mathcal{L} is the kinetic energy and the second term is the opposite of the potential energy. The corresponding full Euler-Lagrange equation $(d/ds)[\partial\mathcal{L}/\partial\dot{\theta}] - \partial\mathcal{L}/\partial\theta = 0$ is the pendulum equation (see equations 4.2 and 6.3):

$$\mu \ddot{\theta} + P \sin \theta = 0 \quad (6.7)$$

But since \mathcal{L} does not depend explicitly on s , a first integral can be obtained directly as $\dot{\theta}\partial\mathcal{L}/\partial\dot{\theta} - \mathcal{L} = \text{const}$:

$$\frac{1}{2} \mu \dot{\theta}^2 - P \cos \theta = \text{const} \quad (6.8)$$

which is the energy of the rod trajectory (equation 4.4), just like equation (6.5) is that of the meniscus trajectory. Alternatively, integrating the pendulum equation with respect to the curvilinear distance s leads to the condition of local torque balance:

$$\mu \dot{\theta} + P(y - y_0) = 0 \quad (6.9)$$

(where the torque is assumed to vanish at altitude y_0), which is the same as equation (6.2).

The present variational approach shows that the energy of the meniscus is a natural function of the altitude y , while that of the rod is expressed in terms of the angle θ . The reason for this discrepancy is essentially that the energy of the rod is unchanged by translation, whereas if the meniscus is translated vertically, the gravitational energy of the liquid is altered. As a consequence, the corresponding Euler-Lagrange equations differ also (see equations 6.2 and 6.7). In fact, the difference between both problems lies essentially in a derivative: equation (6.3), which is the same as the rod Euler-Lagrange equation (6.7), is also the derivative of the meniscus Euler-Lagrange equation (6.2). That is due to the fact that the angle θ is essentially the derivative of the altitude y (more precisely, $\tan \theta = dy/dx$ and $\sin \theta = -dy/ds$).

As a conclusion, although the equilibrium shape of these systems obey the same equation, it is difficult to say that the underlying physics are identical. The energies involved in the two problems are not similar. There is a chance that their dynamics are different. However we will see in next section that they display similar instabilities.

6.2. Rayleigh-Taylor Instability and Buckling Instability.

The well-known Rayleigh-Taylor instability of a liquid and the buckling instability of a compressed rod (due to Euler) almost have a pendulum counterpart. In the present paragraph, we review the first two. We discuss in detail the analogous pendulum instability in the next paragraph.

If the free surface of a liquid (assumed to be horizontal) is submitted to a sinusoidal perturbation $\xi = \delta y \sin(kx)$, its evolution will depend crucially on whether air is above (16-(a)) or below the liquid (16-(b)). Assuming the liquid is initially at rest, a point located within the liquid just beneath the free surface will be accelerated due to the surface deformation: $\ddot{\xi} \propto \mp \rho g \xi - \sigma k^2 \xi$, where the minus (resp., plus) sign corresponds to the situation of figure 16-(a) (resp., b). The first term corresponds to the hydrostatic pressure exerted by the bulk of the liquid, which is stabilizing in case (a) and destabilizing in case (b). The second term is the Laplace pressure exerted by the curved free surface, which is always stabilizing. The evolution can be written as:

$$\ddot{\xi} \propto \rho g \xi [\mp 1 - (ka)^2]. \quad (6.10)$$

Hence, when air is above the liquid, the square bracket is always negative: puddles are

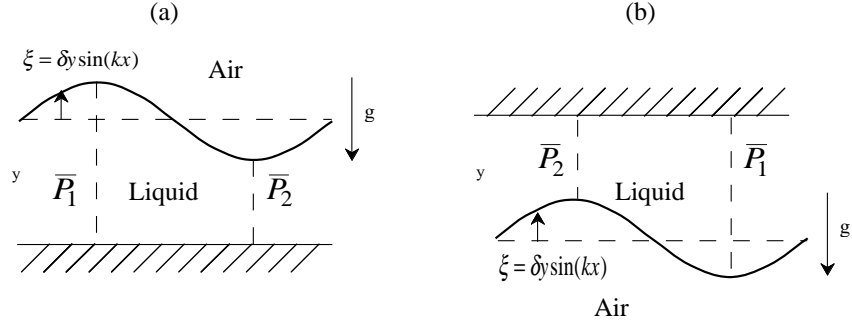


Figure 16. Rayleigh-Taylor Instability: (a) Stable situation when air is above the liquid. (b) Possible unstable situation when air is below the liquid.

stable. In the reverse situation (figure 16-b), the system is stable for wavelengths smaller than $2\pi a$ but becomes unstable when:

$$k.a < \mathcal{O}(1) \quad (6.11)$$

Hence, pendant puddles of extension larger than $2\pi a$ are unstable. This is the Rayleigh-Taylor instability [11].

Let us now turn to a straight rod which is either stretched or compressed with a force P that is aligned with it. The stretched situation is analogous to a drop resting on a solid and is thus always stable. The compressed rod, however, is unstable (buckling was probably first described by L. Euler) when the force exceeds the critical value $P_c = \mu k^2/b$, i.e., when:

$$k.a_e < \sqrt{b} \quad (6.12)$$

where k is the wavenumber of the perturbation (on the order of the inverse rod length) and b is a constant that depends on the boundary conditions [12]. The rod thus buckles when its size is larger than the elastic length a_e . This is therefore directly analogous to the Rayleigh-Taylor instability.

This might be surprising because the analogy we described was restricted to equilibrium shapes and instabilities are a true expression of the dynamics, which are certainly very different. Indeed for a rod, the length of the line is always conserved, and the final state will be a buckled rod, but for an unstable liquid subject to the Rayleigh-Taylor instability, the length of the interface varies at fixed enclosed volume, and the final state is obtained when the liquid has fallen down.

However, the knowledge of all the equilibrium states as a function of a governing parameter is sufficient to understand the dynamics qualitatively. Before the instability is developed, the conserved quantities such as the size x of the liquid interface (which ensures volume conservation) and the length l of the rod are linearly the same. Hence, neutral modes (which are exactly like other equilibrium solutions) are identical in both systems, and so are thus the instability criteria.

6.3. Corresponding pendulum instability?

The pendulum does not display an instability strictly similar to the Rayleigh-Taylor instability for the meniscus or to the Euler buckling instability for the rod described in the last paragraph.

The first, obvious difference is that the situation where the meniscus can display the

Rayleigh-Taylor instability (liquid above air) and the situation where the rod can buckle (compressed state) correspond, via the analogy, to the bottom position of the pendulum, which is unconditionally stable.

A further difference between the pendulum and the meniscus or the rod is that the curvilinear distance s is now turned into the time t : the strict equivalent of a sinusoidal perturbation (wavenumber k) of the rod or the liquid surface is a sinusoidal movement of the pendulum at some angular frequency, ω . This is not transposable as such because the pendulum has no other degree of freedom: if its position is prescribed at all times, the problem becomes pointless. This is in contrast with the liquid surface (or the rod) whose shape can be prescribed at $t = 0$ and which can still evolve freely at later times. For the pendulum, the time t is already the equivalent of the spatial coordinate s . To date, we have not found any setup that would display an equivalent instability. Any suggestion is welcome.

We note that the classical parametric forcing [13] yields another type of instability. The attachment point of the pendulum is vibrated vertically, which amounts to oscillating the parameter g . In this situation, a harmonic oscillator can be excited by a signal at twice its own frequency or at subharmonics thereof. Such a behavior is very different from the ones considered here (Rayleigh-Taylor and buckling). Furthermore, the pendulum is non-linear and its resonance frequency depends on the amplitude, hence the frequency of a weak parametric forcing should be adjusted dynamically in order to bring the pendulum to large amplitudes.

6.4. Flexible sheet enclosing a liquid

Earlier in this section, we showed that the energy of the rod and that of the meniscus cannot be written in the same fashion. Here, we consider a system that somehow interpolates between the meniscus and the rod.

In the two-dimensional geometry, the free surface of the liquid transmits a force which is tangential and of constant amplitude, and upon bending, it is able to support the pressure of the liquid which is normal. By contrast, due to its bending rigidity, the rod transmits forces of arbitrary orientations and transmits also torques, but it is not subjected to any external stresses other than the end-loading forces and torques.

In order to combine these features, we here consider a flexible membrane (with a finite bending rigidity μ) with air on one side and a liquid on the other side. We suppose that the membrane is inextensible [14].

The stresses in the membrane are then given by:

$$\dot{\Gamma} = -P.n \quad (6.13)$$

$$\dot{P} = p.n \quad (6.14)$$

$$\Gamma = -\mu\dot{\theta} \quad (6.15)$$

$$\dot{p} = -\rho g \sin \theta \quad (6.16)$$

where P and Γ are the usual force and torque transmitted along the membrane (curvilinear abscissa s), and where n and u are the unit vectors normal and tangent to the membrane, respectively. The first two equations express the local torque (see equation 4.1) and force balances, the third equation reflects the bending elasticity of the membrane and the fourth gives the hydrostatic pressure in the liquid.

From equations (6.13) and (6.15), the normal component of the transmitted force can clearly be expressed as

$$P.n = \mu\ddot{\theta} \quad (6.17)$$

Using the derivatives of the unit vectors $\dot{u} = \dot{\theta}n$ and $\dot{n} = -\dot{\theta}u$, the tangent component

of the force can be derived from $d(P.u)/ds = \dot{P}.u + \dot{\theta}P.n = 0 + \mu\ddot{\theta}\dot{\theta}$:

$$P.u = \frac{1}{2}\mu\dot{\theta}^2 - A \quad (6.18)$$

where A is a constant (in the limit of vanishing bending rigidity, it is equivalent to the surface tension σ). From the expression of $P.n$:

$$\mu\theta^{(3)} = d(P.n)/ds = \dot{P}.n - \dot{\theta}P.u \quad (6.19)$$

$$= p - \frac{1}{2}\mu\dot{\theta}^3 + A\dot{\theta} \quad (6.20)$$

Finally, the shape of the membrane is described by a fourth order ordinary differential equation:

$$\mu\theta^{(4)} + \frac{3}{2}\mu\ddot{\theta}\dot{\theta}^2 - A\ddot{\theta} + \rho g \sin \theta = 0 \quad (6.21)$$

The unknown parameter A and the solution to the equation are determined from five initial conditions at $s = 0$: the angle θ , the pressure p , the applied torque $\Gamma(0) = -\mu\dot{\theta}(0)$ and both components of the applied force $P(0)$.

$$A = \frac{1}{2}\Gamma^2(0)/\mu - P(0).u(0) \quad (6.22)$$

$$\theta(0) = \text{specified} \quad (6.23)$$

$$\dot{\theta}(0) = -\Gamma(0)/\mu \quad (6.24)$$

$$\ddot{\theta}(0) = P(0).n(0)/\mu \quad (6.25)$$

$$\theta^{(3)}(0) = p(0)/\mu + \Gamma(0)P(0).u(0)/\mu^2 \quad (6.26)$$

The full equation (6.21) clearly reduces to the meniscus equation (3.6) in the limit of vanishing bending rigidity μ :

$$-A\ddot{\theta} + \rho g \sin \theta = 0 \quad (6.27)$$

In a region where the membrane spans only a small vertical distance, the pressure p is essentially constant and the shape is described by equation (6.20) which does not depend explicitly on θ (because the problem is then invariant by rotation). If, furthermore, the pressure is negligible, then this equation reduces to:

$$\theta^{(3)} + \frac{1}{2}\dot{\theta}^3 - \frac{A}{\mu}\dot{\theta} = 0 \quad (6.28)$$

One can check that the usual rod conformation (see equation 4.4) specified by the initial condition (6.23) and by:

$$\frac{1}{2}\dot{\theta}^2 + k \cos[\theta - \alpha] - \frac{A}{\mu} = 0 \quad (6.29)$$

is then duly the solution of equation (6.28) with the specified initial conditions, provided that k and α are chosen in such a way that:

$$-k \cos[\alpha - \theta(0)] \equiv P(0).u(0)/\mu \quad (6.30)$$

$$-k \sin[\alpha - \theta(0)] \equiv P(0).n(0)/\mu \quad (6.31)$$

In other words, α is the oriented angle between the tangent vector u and the applied force P , and $k = -|P|/\mu$.

In general, the full equation (6.21) does not have pendulum-like solutions: such a solution is only valid locally. For instance, suppose that the flexible membrane is clamped on both ends at the same altitude, at a fairly small distance from one another, and that the liquid

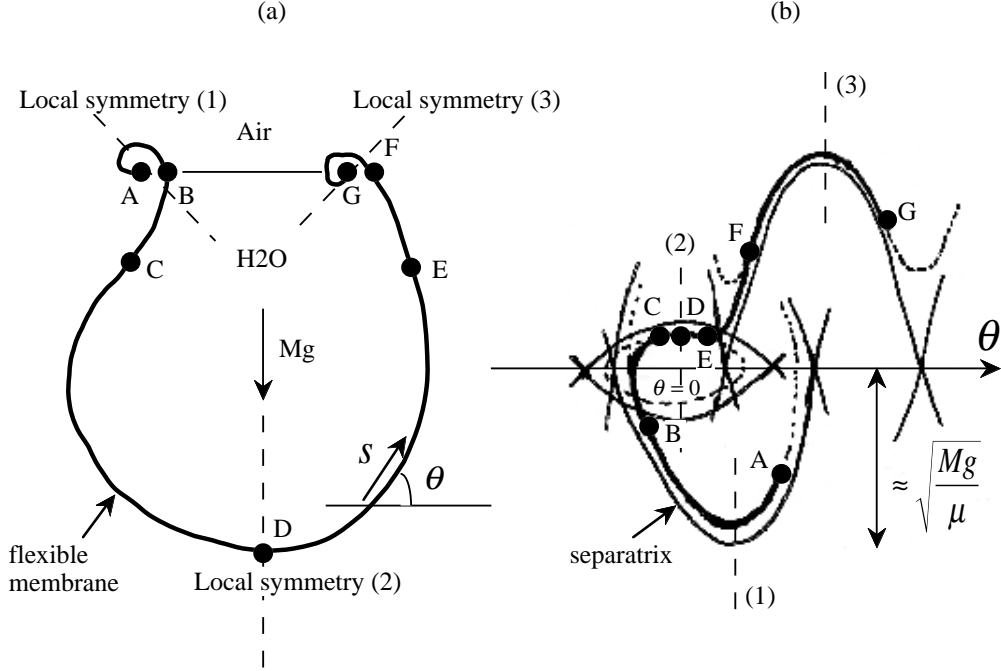


Figure 17. (a) Inextensible, flexible membrane with finite bending rigidity enclosing a liquid. (b) Trajectory of the flexible membrane in the $[\theta, \dot{\theta}]$ diagram. It interpolates between a meniscus-like region (with a large characteristic length-scale) and a rod-like region near the clamped ends of the membrane (with a small length-scale).

is poured into the resulting hollow-shaped membrane (see figure 17-(a)). On the large scale, the curvature of the membrane is small and if the bending rigidity μ is not too large, the shape is simply that of a pendant drop, according to equation (6.27). Near the clamped ends of the membrane, however, depending on the orientation that is imposed, the curvature can be quite high. Since the pressure of the liquid is negligible there, we recover a rod-like conformation, see equation (6.29). The characteristic length scales of these two regions of the membrane are not the same, so that on a $[\theta, \dot{\theta}]$ diagram, the trajectory of the membrane goes from a first pendulum-like solution with one length scale to a second such solution with another length scale (see figure 17-(b)). In the crossover region, both the membrane bending rigidity and the liquid pressure are important and the full equation (6.21) does not reduce to a pendulum equation.

For special initial conditions, however, even the full equation (6.21) has a pendulum-like solution. Indeed, one can show that the trajectory defined by the initial condition (6.23) and by:

$$\frac{1}{2}\dot{\theta}^2 + k \cos \theta + \frac{\rho g}{\mu k} - \frac{A}{\mu} = 0 \quad (6.32)$$

is the solution of equation (6.28) if:

$$k \cos[\theta(0)] \equiv -P(0).u(0)/\mu - \frac{p(0)}{\Gamma(0)} \quad (6.33)$$

$$\text{and } k \sin[\theta(0)] \equiv +P(0).n(0)/\mu \quad (6.34)$$

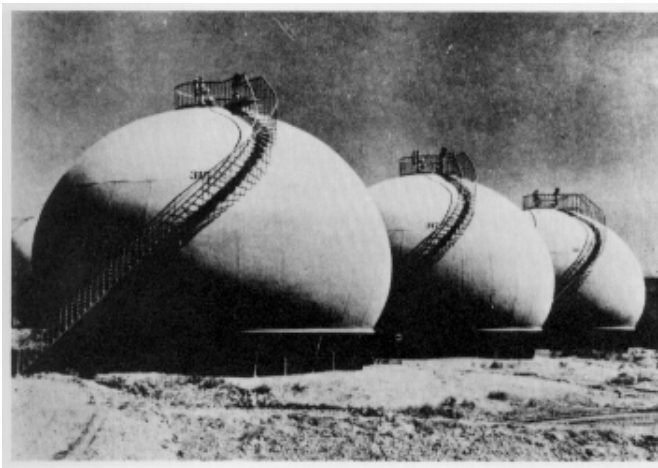


Figure 18. Storage tanks with metallic staircases for maintenance (from McMahon and Bonner, *On Size and Life*). They are called Hortonspheroids and generally contain hydrocarbons under pressure. Their shape closely follows that of liquid drops such as those presented on figure 3, although discrepancies are due to other real engineering issues such as the transition of forces at the interface with the foundation. Photo and comments: courtesy of Chicago Bridge & Iron Company.

These two equations yield a unique value of k , provided that the initial conditions at $s = 0$ obey the following:

$$P(0).n(0) \cos[\theta(0)] + \{P(0).u(0) + p(0)\mu/\Gamma(0)\} \sin \theta(0) = 0 \quad (6.35)$$

To conclude this section, let us mention that containers used to store large amounts of liquid under pressure (see figure 18) have essentially the same shape as liquid drops resting on a solid (figure 3), as pointed out by McMahon and Bonner [15] in their beautiful book *On Size and Life*. This may seem surprising since the interface between the stored liquid and the air (i.e., the container walls) is not precisely a free surface ! The steel walls can transmit forces and torques, and as was described above, the shape of the container could therefore be very different from the pendulum equation. In fact, the shape of the container (i.e., in its initial, unloaded state) was designed to match that of a drop for a precise reason: at least when the container is full of liquid at the appropriate pressure, the forces are oriented tangentially within the walls [16] and their intensity is the same everywhere, just like surface tension. This very clever design thus requires walls of essentially constant thickness. Moreover, the absence of transmitted torques in a full container reduces the risks of additional wall bending and fatigue. The bottom part of the real shape, however, is slightly different from that of a liquid drop due to various engineering issues and in particular the need for an appropriate transmission of stresses between the walls of the tank and the foundation.

7. Historical note

The present work started independently in Marseille [17] and in Paris [18],[19],[20] until two of the authors met for dinner, one ocean away from their home country. They happened to talk about a knife, a glass of water and a pair of laces, and all at once they knew that they had been thinking about the very same analogy for several months

already. They wish to dedicate this work to all those who certainly have also pondered this analogy over the years.

A similar analogy was drawn by G. I. Taylor and A. A. Griffith in a series of three papers [23]. The height profile $h(x, y)$ of a soap film attached to a planar contour and subjected to a small pressure difference obeys $(\partial_x^2 + \partial_y^2) h = \text{const}$. The same equation is obeyed by a function which describes the shear stresses in the section of a twisted bar, the contour of the section being the same as that of the soap film. This analogy was used for determining the torques and resistance of airplane wings and was motivated by the developments of aeronautics during the First World War.

8. Acknowledgements

We wish to thank Howard Stone who made the conversation mentioned above possible during the meeting of the Division of Fluid Dynamics of the American Physical Society in Washington in November 2000. We are also grateful to Michael Brenner for bringing reference [9] and the beautiful papers [23] to our attention.

REFERENCES

- [1] D'Arcy W. Thompson 1992 On Growth and Form In Dover Publications, Inc., New York.
- [2] A.M. Turing 1952 The chemical basis of morphogenesis, In Phil. Trans. Roy. Soc. (London) 237 pp. 37–72.
- [3] G.I. Barenblatt 1987 Dimensional analysis, In Gordon and Breach Science Publishers
- [4] S. Douady, Y. Couder 1993 La physique des spirales végétales, In La Recherche 24 pp. 26–35.
- [5] L. Mahadevan 1998 In Nature 392 pp. 140.
- [6] L. Mahadevan 2000 In Nature 403 pp. 502.
- [7] F.M. Orr, L.E. Scriven and A.P.Rivas 1975 Pendular rings between solids: meniscus properties and capillary force In Journal of Fluid Mechanics 67 pp. 723–743.
- [8] Gillette, Dyson 1971 In Chemical Engineering Science 2 pp. 44.
- [9] S.R. Majumdar, D.H. Michael 1976 The equilibrium and stability of two dimensional pendent drops, In Proc. R. Soc. Lond. A. 351 pp. 89–115.
- [10] L. Landau, E. Lifchitz 1986 Physique Théorique : Mécanique des fluides. Mir.
- [11] S. Chandrasekhar 1981 Hydrodynamic and hydromagnetic stability. Dover.
- [12] L. Landau, E. Lifchitz 1986 Physique Théorique : Théorie de l'élasticité Mir.
- [13] L. Landau, E. Lifchitz 1986 Physique Théorique : Mécanique Mir.
- [14] An inextensible membrane is simply a very thin membrane made from a material with a very high elastic modulus. We use this case for simplicity, but without losing of generality. Indeed, the degree of stretching varies along the membrane since the force transmitted in the tangent direction varies. But as long as stretching is weak, it does not affect the bending rigidity. As a result, including weak stretching only amounts to imposing different integral conditions such as the length of the membrane.
- [15] A. McMahon, J.T. Bonner 1983 On Size and Life In Scientific American Library, Freeman and Co. New York.
- [16] The transmitted forces are tangent to the walls (i.e., $P.n = 0$) because the rounded shape of the container is its initial, stress-free state. By contrast, the initial state of the flexible membrane is the straight conformation.
- [17] B. Roman 2000 De l'Elastica aux plaques plissées In Thèse de l'Université de Provence.
- [18] C. Gay 1999 In La Recherche 325 pp. 99.
- [19] C. Gay 2000 In La Recherche 337 pp. 94.
- [20] C. Gay 2001 In La Recherche 340 pp. 24.
- [21] KIRCHHOFF 1944 A Treatise on the Mathematical Theory of Elasticity In Love Dover.
- [22] J.C.MAXWELL In Encyclopedia Britannica, 9th. ed., 1878, New York. art. "Capillary action".

- [23] G. I. Taylor and A. A. Griffith 1917 In Reports and Memoranda of the Advisory Committee for Aeronautics 333, 392, 399.